ELSEVIER

Journal of Nuclear Materials 273 (1999) 302–309

journal of nuclear materials

www.elsevier.nl/locate/jnucmat

Depth profiles of damage accumulation in UO_2 and $(U,Gd)O_2$ pellets irradiated with 100 MeV iodine ions

K. Nogita [a,*], K. Hayashi [b], K. Une [a], K. Fukuda [b,1]

[a] *Nippon Nuclear Fuel Development Co., Ltd., Higashi-ibaraki-gun, 2163, Narita-cho, Oarai-machi, Ibaraki-ken, 311-1313, Japan*
[b] *Japan Atomic Energy Research Institute, Tokai-mura, Naka-gun, Ibaraki-ken, 319-1195, Japan*

Received 17 August 1998; accepted 7 February 1999

Abstract

To study the initial defect formation and accumulation process during fission events, sliced pellet specimens of UO_2 and $(U,Gd)O_2$ were irradiated at ambient temperatures below 200°C, with 100 MeV iodine ions over a fluence range of $1.0 \times 10^{18} - 2.0 \times 10^{19}$ ions/m^2. The surface of the specimens was analyzed by scanning electron microscopy (SEM) and X-ray diffractometry (XRD), and then the depth profiles of incident iodine ions and defect clusters were measured by secondary ion mass spectrometry (SIMS) and transmission electron microscopy (TEM), respectively. Lattice parameter change, which is associated with point defect accumulation, increased with ion fluence. Defect clusters of dislocations and dislocation loops were recognized, and their depth profiles were in good agreement with the calculated damage profile. These profiles of iodine ions and dislocation loops in both UO_2 and $(U,Gd)O_2$ were discussed in terms of inelastic and elastic collisions.

1. Introduction

Ceramic UO_2 and $(U,Gd)O_2$ fuel pellets are widely used in light water reactors (LWRs). During irradiation, fission of ^{235}U generates median heavy and light fission fragments (mass numbers: 137 and 96) of about 65 and 95 MeV energies [1]. Fission tracks in random directions into the matrix, with a deposition of large energy through inelastic and elastic collisions [1,2], form lattice defects, and then bring about microstructural change such as the 'rim effect' in the peripheral region of high burnup LWR fuel pellets [3,4]. To study the initial defect formation process along fission tracks, ion bombardment by a high energy accelerator is a powerful method. In previous papers, Hayashi et al. [5,6] scrutinized the lattice parameter change of UO_2 irradiated with 100, 200 and 300 MeV iodine ions as functions of fluence and the electronic energy deposition at the specimen surface. In the present study, 100 MeV iodine ions were irradiated to study the radiation damage in the fission fragment energy region. Particular emphasis was put on the surface morphology, and the depth profiles of defects and microstructure changes in UO_2 and $(U,Gd)O_2$ pellets.

2. Experimental

2.1. Specimens

The specimens used were sintered UO_2 and UO_2–10wt%Gd_2O_3 disks (diameter: 10 mm, thickness: 1 mm) with average grain sizes of 61 and 53 μm, respectively. The densities of the specimens were 96.4% of the theoretical density for UO_2 and 96.1% for $(U,Gd)O_2$. The specimen disks were polished with emery paper and diamond paste of about 1 μm particle size. The specimens were subsequently annealed in flowing $N_2/8\%H_2$ gas at 1500°C for 2 h, so as to remove any surface damage due to polishing, although no change due to polishing had been detected in the lattice parameter obtained by X-ray diffractometry (XRD) and scanning electron microscopy (SEM) observations.

* Corresponding author. Tel: +81-29 266 2131; fax: +81-29 266 2589; e-mail: nogita@nfd.co.jp

[1] Present address: International Atomic Energy Agency, Wagramerstrasse 5, P.O. Box 200, A-1400 Vienna, Austria.

0022-3115/99/$ – see front matter
PII: S0022-3115(99)00048-3

Table 1
Details of irradiation conditions

Specimen	Grain size (μm)	Density (%TD)	Fluence (ions/m^2)
UO_2	61	96.4	1.0×10^{18}
			2.0×10^{18}
			5.0×10^{18}
			2.0×10^{19}
(U,Gd) O_2	53	96.1	1.0×10^{18}
			2.0×10^{18}
			5.0×10^{18}
			2.0×10^{19}

2.2. Irradiation

Irradiation was done with 100 MeV $^{127}I^{7+}$ ions at ambient temperatures using the Tandem Accelerator of the Tokai Establishment of the Japan Atomic Energy Research Institute (JAERI). Ion beam fluences were 1.0×10^{18}–2.0×10^{19} ions/m^2. Ion-irradiated regions were about 5 mm in diameter.

Detailed irradiation conditions of each specimen are summarized in Table 1. In order to suppress the effect of ion beam heating at the beam incidence side surface, the rear side of the specimen was cooled by water that was kept at about 20°C. The temperature at the beam-incidence side surface was monitored during irradiation by a low-temperature infrared pyrometer with a PbS sensor, and it was lower than 200°C, which is the detection limit of the pyrometer. The ion fluence was measured by a current integrator, and the time-averaged ion flux was evaluated from the fluence. The pressure in the vacuum target chamber was kept below 3×10^{-3} Pa. The experimental procedure was essentially the same as described in Refs. [5,6].

2.3. Examinations

Irradiated and unirradiated surface regions of the specimens were observed by SEM. The magnifications of SEM were 100× and 1000×.

Lattice parameters at the specimen surfaces were measured by X-ray diffraction (XRD) with a Cu Kα radiation. The X-ray beam diameter was 1 mm and focused on the center of the ion-irradiated region which was about 5 mm in diameter. The lattice parameter was obtained by least-squares calculations of the five diffraction lines between 90° and 130° in 2θ. The penetration depth of the X-rays into the UO_2 specimen was estimated to be about 2 μm [7].

Depth profiles of irradiated iodine ions were measured by a secondary ion mass spectrometer (SIMS) with the primary oxygen ions (accelerate voltage: 15 kV, beam current: 100 nA, beam diameter: 50 μm). Concentration of the implanted iodine ions was normalized by that of oxygen ions in the UO_2 or $(U,Gd)O_2$ matrix. The depth from the surface was evaluated by taking the relation between the sputtering time of the primary oxygen ions and the depth measured by a roughness meter. The relation between the sputtering time, T (min), and the depth, D (μm), was obtained as $D = 0.0295$ T for the present experimental conditions.

For cross-sectional transmission electron microscopy (TEM) observations, small cubic pieces, about 1 mm on a side, were cut from the disk pellet specimens in the ion-irradiated region, using a cross cutter. The sample pieces were embedded perpendicular to the irradiated surface [8,9] in inorganic cement within a 3 mm diameter stainless steel washer and ground to a thickness of about 100 μm. Thinning was finished by ion milling with 5 keV argon ions. Cross-sectional images from the surface to about 10 μm depth were taken with a 200 kV TEM.

3. Results and discussion

3.1. Surface morphology and lattice parameter change

Ion-irradiated regions of about 5 mm in diameter were easily visible for all the disks. Fig. 1(a) shows a low magnification SEM micrograph of the surface for a UO_2 disk irradiated to 2.0×10^{19} ions/m^2. Magnified SEM micrographs of unirradiated and irradiated regions, which correspond to (b) and (c) in Fig. 1(a), are shown in Fig. 1(b) and (c), respectively. These SEM images of the specimen surface were taken perpendicular to the direction of the incident ions. As shown in Fig. 1(c), three types of changes in the surface morphology, namely, surface smoothing, protrusion and crater formations are observable. Similar smoothing and protrusion formation can be seen in the irradiated region of all UO_2 and $(U,Gd)O_2$ specimen disks. Strong ion-fluence dependence on surface smoothing cannot be observed for either UO_2 or $(U,Gd)O_2$ specimens. The smoothing and protrusion phenomena are similar to those which had been observed in UO_2 [5] irradiated with 100 MeV iodine ions.

Fig. 2(a) shows the depth profiles of the nuclear and electronic energy depositions and the incident iodine ion

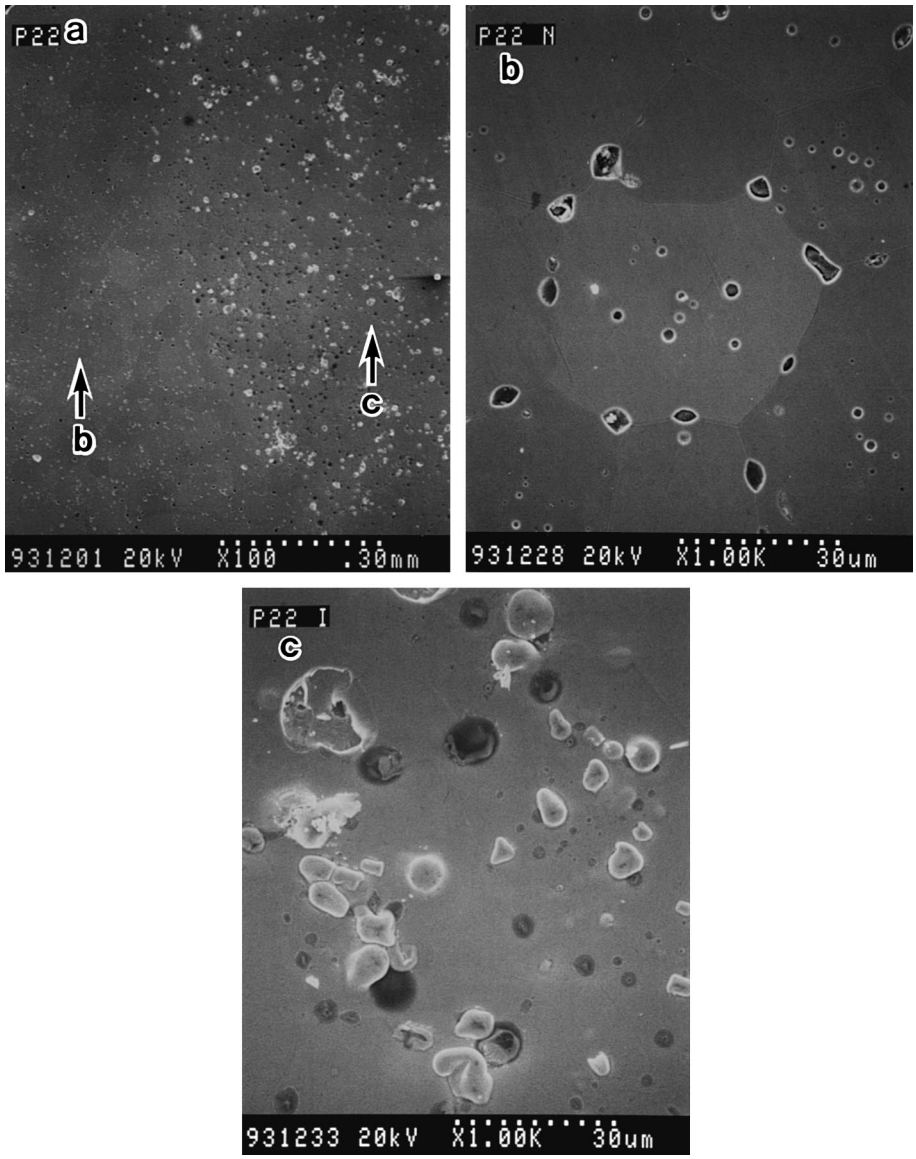

Fig. 1. SEM micrographs of the surface for a UO_2 disk irradiated to 2.0×10^{19} ions/m^2; (a) low magnification (100×); (b) unirradiated region (1000×); (c) irradiated region (1000×).

concentration in UO_2 calculated by the TRIM code [10]. Two different phenomena take place along the fission tracks in the UO_2 crystal. First, at the beginning of the fission fragment range, the energy is mainly lost by electronic excitation. The formation of a thermal spike is due to a high energy deposition which is mainly attributed to inelastic (electronic) collisions. The energy deposition is the highest at the beginning of the track. On the other hand, that due to elastic (nuclear) collisions dominates near the end of the track. The stopping power of the 100 MeV iodine ions due to the electronic process was estimated to be about 20 keV/nm [10] at the surface of the disk. The large energy deposition at the surface might contribute significantly to heating of the lattice. On the other hand, at such a high ion energy, displacement damage at near-surfaces caused by nuclear collisions is very little, compared with that in the neighborhood of the projected range peak. The fission damage in nuclear fuels has been explained mainly by models of the thermal spike [11–13] and Coulomb explosion spike [14,15]. For the thermal spike model, a volume of $10^{-22} - 10^{-21}$ m^3 along the ion track is heated up to 2000–3000°C for about 10^{-11} s [13]. Fig. 2(b) indicates the calculation results of radial temperature

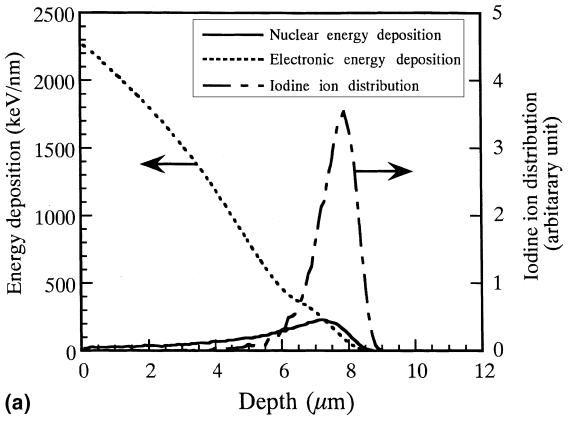

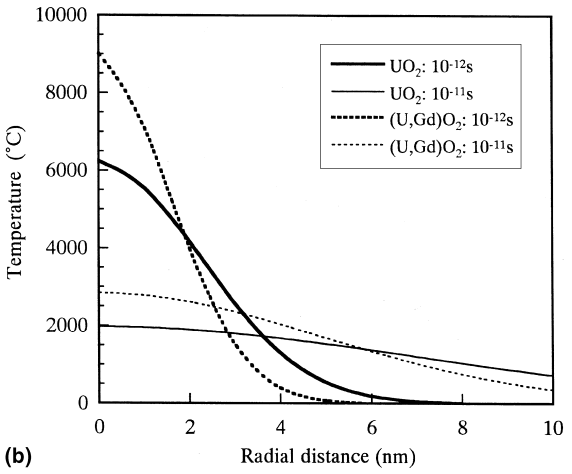

Fig. 2. (a) Depth profiles of electronic and nuclear energy depositions and ion distribution calculated by TRIM code. (b) Calculated temperature distributions around the thermal spike in UO_2 and $(U,Gd)O_2$.

distributions along the thermal spike in UO_2 and $(U,Gd)O_2$. Assuming that the thermal diffusion coefficients of 1.2×10^{-6} and 2.5×10^{-6} m^2/s at 200°C for UO_2 and UO_2–10wt%Gd_2O_3 [16], respectively, can be used in this rapid transient as a rough estimate, the energy transferred to the center of the fission track can be converted to temperature increases of about 6000°C and 9000°C in 10^{-12} s, and 2000°C and 3000°C in 10^{-11} s, respectively. This suggests that a part of the volume along the track might melt or evaporate on a very short time scale, even though the macroscopic surface temperature is lower than 200°C. Thus, the changes of surface morphology such as surface smoothing and protrusion formation observed in the present experiment would be mainly attributed to thermal damage, not to displacement damage.

Lattice parameter change of UO_2 and $(U,Gd)O_2$ is plotted as a function of the ion fluence in Fig. 3. This figure indicates that the lattice parameter change in-

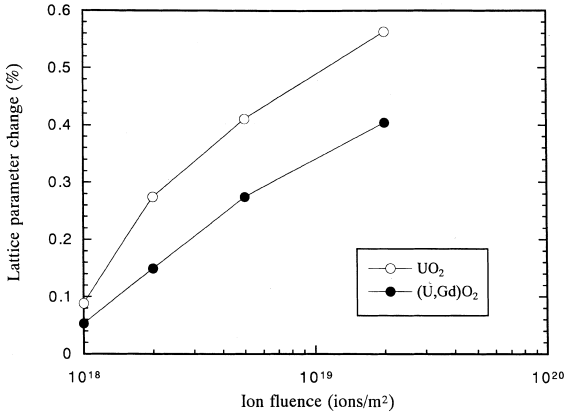

Fig. 3. Lattice parameter change of UO_2 and $(U,Gd)O_2$ specimens as a function of the ion fluence.

creases with increasing ion fluence, and that the change is higher for UO_2 than for $(U,Gd)O_2$ specimens. The values for UO_2 and $(U,Gd)O_2$ reach 0.56 and 0.4%, respectively, at 2×10^{19} ions/m^2. The lattice parameter of oxide fuels with the fluorite structure is known to be affected by the oxygen to metal atom ratio (O/M), dissolution of solid fission products (FPs), and accumulation of irradiation-induced lattice defects [16]. The accumulation of radiation defects increases the lattice parameter, while the increase in O/M ratio and the dissolution of soluble FPs decrease it. Since the penetration depth of X-rays into a specimen is about 2 μm from the surface [5] and almost all incident ions are calculated to be accumulated at around 7 μm away from the surface, the direct effect of incident iodine atoms on the lattice expansion at the surface would be negligible. Therefore, the lattice parameter change in the present study is considered to be due to the accumulation of point defects [17].

There are several reports on the lattice parameter change due to fission events [18–20]. The lattice parameter initially rises rapidly with fission fluence, passes through the maximum at about 1.0×10^{23} fissions/m^3 and falls to about half of its maximum value by 2.0×10^{24} fissions/m^3. This characteristic curve of lattice parameter change is interpreted as an initial production of a supersaturated concentration of interstitial type point defects followed by nucleation and growth of defect clusters as a dislocation loop. Assuming the distance travelled by a fission fragment is 10 μm in the above reports, fission fluence of 1.0×10^{23} fissions/m^3 is converted to two-dimensional fluence of 1.0×10^{19} fissions/m^2. This assumption indicates that the lattice parameter change in the present results (ion-fluence range: 1.0×10^{18}–2.0×10^{19} ions/m^2) is caused by accumulation of interstitial type point defects. It is noted in Fig. 3 that point defects are accumulated even in the inelastic collision governed region, and that the defect

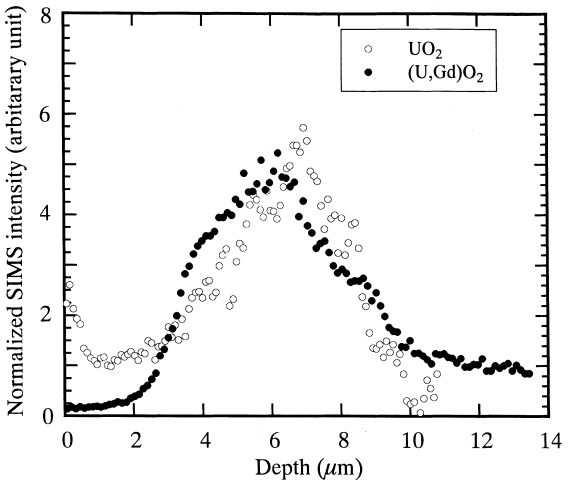

Fig. 4. Depth profiles of irradiated iodine ions.

concentration is lower in $(U,Gd)O_2$ than in UO_2 specimens at the near-surface region. One of the possible reasons for this lattice parameter change is the temperature difference in the thermal spike. As shown in Fig. 2(b), the local temperature of the thermal spike in the $(U,Gd)O_2$ specimen is higher than that in the UO_2 specimen in the same period, since the thermal conductivity of the former is about 2/3 of the latter. Consequently, a greater amount of lattice defects would remain in UO_2 based on the thermal spike model.

3.2. Depth profiles of irradiated iodine ions and microstructural change

Depth profiles of iodine ion concentration, which were measured by SIMS, in UO_2 and $(U,Gd)O_2$ specimens both irradiated to a fluence of 5.0×10^{18} ions/m^2 are shown in Fig. 4. The profile is relatively broader in $(U,Gd)O_2$ than in UO_2 with the former having a peak at 6–7 μm depth. The overall features of the profile are in better accord with the TRIM calculation results of the nuclear energy deposition profile shown in Fig. 2(a) (peak depth: 7 μm) than the incident iodine ion concentration profile (8 μm). As depicted in Fig. 2(b), the calculated local temperature at the thermal spike in the $(U,Gd)O_2$ specimen is higher than that in the UO_2 specimen in the same period. Therefore, diffusion of iodine ions along the thermal spike is expected to be more enhanced in the $(U,Gd)O_2$ specimen.

Fig. 5 shows a cross-sectional TEM image of a UO_2 specimen (ion fluence: 2×10^{18} ions/m^2). During the sample preparation, the region from the surface to 4 μm was lost by grinding. Therefore, the surface of this image corresponds to 4 μm away from the ion-irradiated surface. Tangled dislocations are distributed in the region of 4–7 μm, having the maximum density at around 5–6.5 μm from the surface. These tangled dislocations are expected to be a result of dislocation loop growth by climb motion [21,22]. The peak depth for the dislocation density (5–6.5 μm) is shallower than the calculated peak (6–7 μm, see Fig. 3(a)) of the nuclear energy deposition. At depths greater than 7 μm, no dislocations or dislocation loops are observed.

A low magnification cross-sectional TEM image of a $(U,Gd)O_2$ specimen (ion fluence: 2.0×10^{19} ions/m^2) is shown in Fig. 6. The images marked (a)–(d) in Fig. 6 correspond to the higher magnification images in Fig. 7(a)–(d), respectively ((a): 0–1.4 μm, (b): 3 μm, (c): 5 μm, (d): 7 μm from the surface). Elliptical dislocation loops are recognized in the near-surface region in Fig. 7(a). The longitudinal direction of the dislocation loops is perpendicular to the surface, i.e., in good agreement with the ion-irradiated direction.

Much TEM work has been performed on low burnup UO_2 with lower irradiation temperature between 50°C and 100°C by Whapham alone and with Shelden [21,22]. By using the $g \times b = 0$ analysis, dislocation loops generated by fission events were found to be the interstitial type on {1 1 0} planes and to have the $b = 1/2[1\ 1\ 0]$ Burgers vector. Since the loops never showed any stacking fault contrast, they were considered to be perfectly prismatic. With increasing burnup, the dislocation loops increased in size until they coalesced with each other forming a tangled dislocation network. The pres-

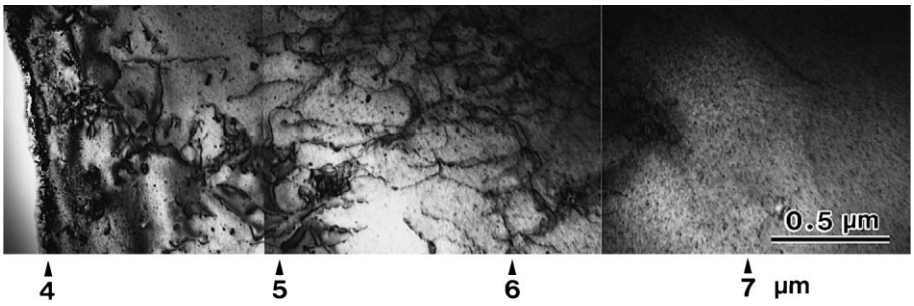

Fig. 5. A cross-sectional TEM image of UO_2 specimen (ion fluence: 2.0×10^{18} ions/m^2).

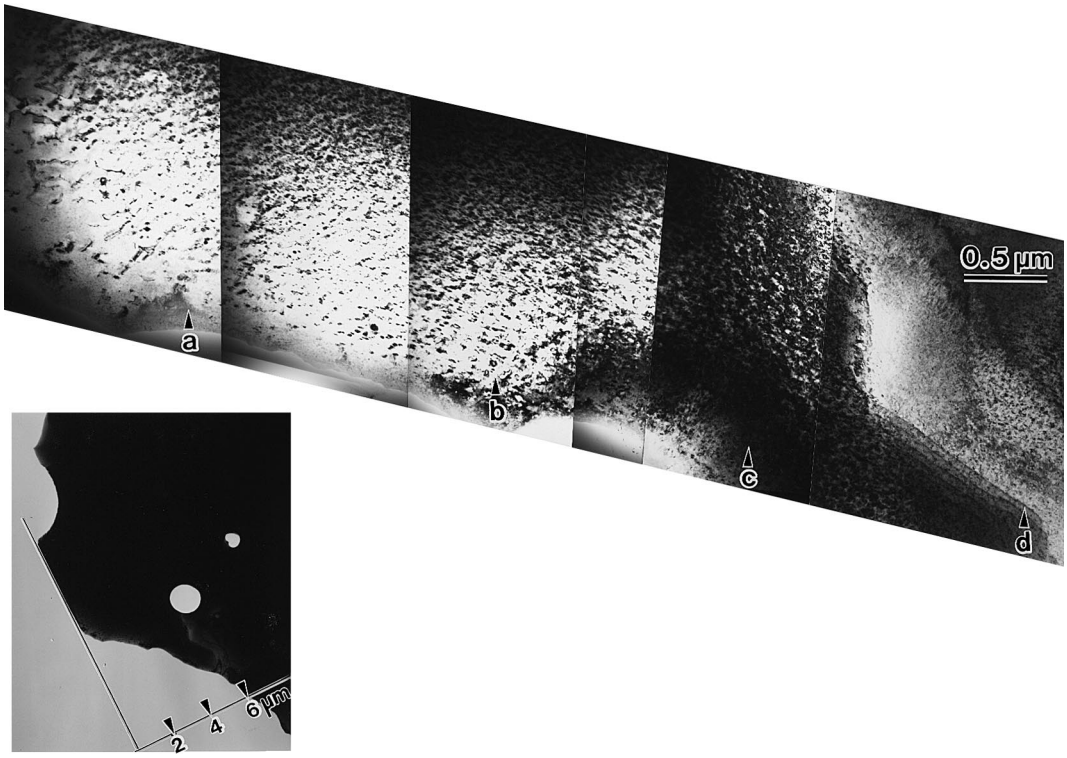

Fig. 6. Low magnification cross-sectional TEM image of $(U,Gd)O_2$ specimen (ion fluence: 2.0×10^{19} ions/m^2).

ent TEM results of dislocation loops and tangled dislocations reasonably correspond to the results of reported features of dislocations.

Depth profiles of the average diameter and number density of dislocation loops for a $(U,Gd)O_2$ specimen irradiated to 2.0×10^{19} ions/m^2 are shown in Fig. 8. The loop diameter is the largest at the surface region, which can be explained by two different mechanisms. One is the thermal spike-enhanced diffusion of defects as discussed in Section 3.1, namely the diffusion was enhanced by the large electronic energy deposition at the surface [14,15]. The other mechanism is the increase in the point defect recombination rate due to ionization-induced diffusion mentioned by Zinkle [23]. Dislocation loops are distributed in the region from the surface to 8 μm with the maximum density at around the 4 μm region from the surface.

4. Conclusions

Sliced pellets of UO_2 and $(U,Gd)O_2$ were irradiated at ambient temperatures below 200°C, with 100 MeV iodine ions over a fluence range of 1.0×10^{18}–2.0×10^{19} ions/m^2. The changes in surface morphology and the depth profiles of incident ions and defects in these pellets were studied by SEM, XRD, SIMS and TEM. The results were summarized as follows:

1. The UO_2 and $(U,Gd)O_2$ specimen surfaces showed a melting-like morphology, namely smoothing and formation of protrusions and craters.
2. The lattice parameter increased with increasing ion fluence, and reached values of 0.56% and 0.4% at 2×10^{19} ions/m^2 in UO_2 and $(U,Gd)O_2$, respectively.
3. The depth distributions of implanted iodine ions had peaks at around 6–7 μm from the surface.
4. The depth distributions of dislocation loops and tangled dislocations peaked at around the 5–6.5 μm region from the surface in UO_2 and around the 4 μm region from the surface in $(U,Gd)O_2$, respectively.

Acknowledgements

The authors are indebted to Messrs. H. Masuda, A. Ouchi and M. Imamura of Nippon Nuclear Fuel Development Co., Ltd. (NFD), and Messrs. H. Kikuchi, T. Shiratori, S. Ichikawa, K. Tsukuda, C. Kobayashi, T. Yoshida and members of the Accelerator Division of the Japan Atomic Energy Research Institute (JAERI) for their assistance in the Tandem Accelerator experiments. They are also grateful to Drs. K. Minato,

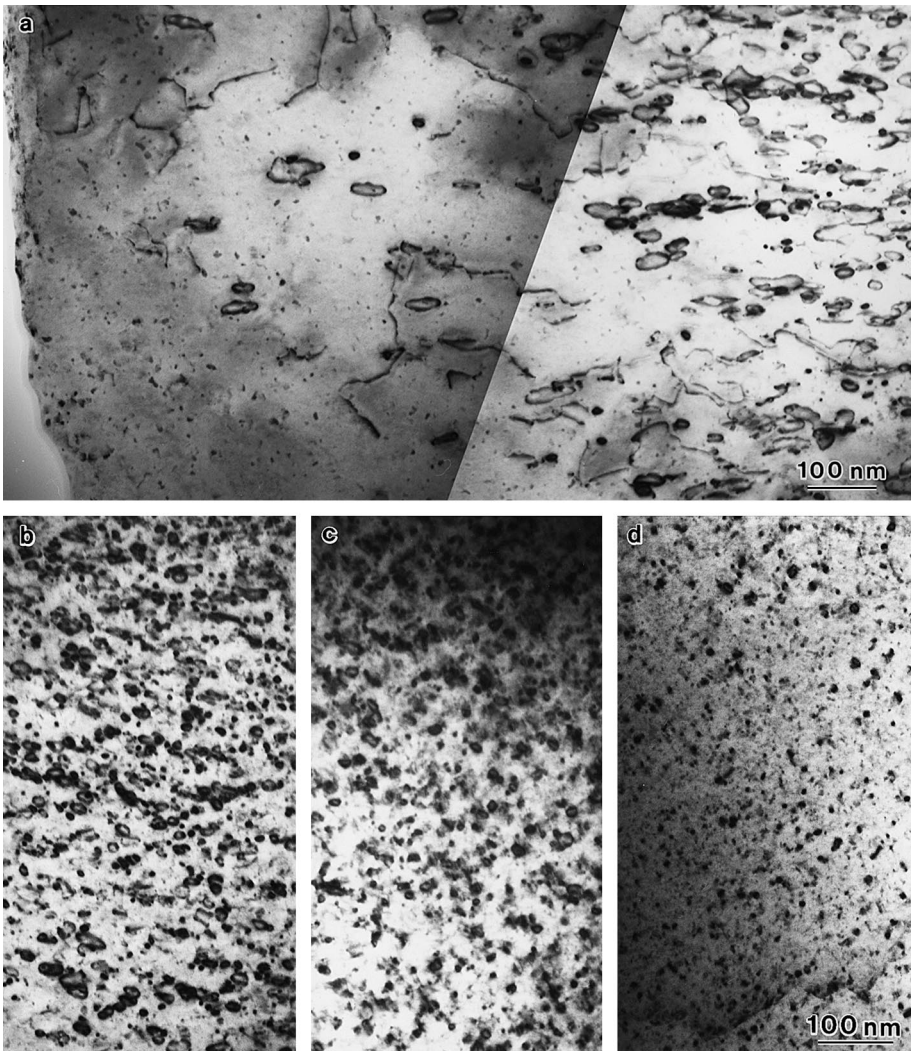

Fig. 7. (a) Cross-sectional TEM images of $(U,Gd)O_2$ specimen (0–1.4 μm from the surface). (b)–(d) Cross-sectional TEM images of $(U,Gd)O_2$ specimen ((b): 3 μm, (c): 5 μm, (d): 7 μm from the surface).

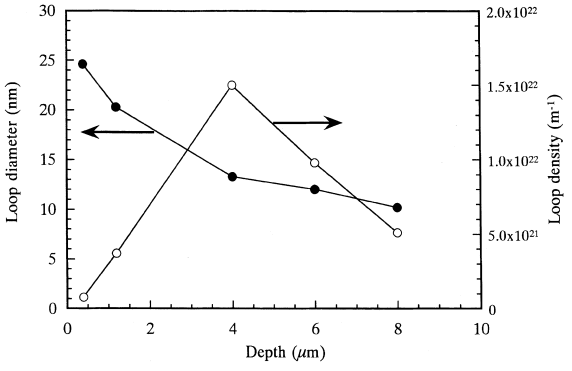

Fig. 8. Depth profiles of average diameter and density of dislocation loops for $(U,Gd)O_2$ specimen irradiated to 2.0×10^{19} ions/m^2.

T. Ogawa and Y. Suzuki of JAERI for helpful discussions and Dr. M. Hoshi and T. Muromura of JAERI for their encouragement.

References

[1] D.R. Olander, Fundamental Aspects of Nuclear Reactor Fuel Elements, Ch. 17, Technical Information Center, Springfield, VA, TID26711-P1 (1974).
[2] Hj. Matzke, Radiat. Eff. 64 (1982) 3.
[3] K. Nogita, K. Une, Nucl. Instrum. and Meth. B 91 (1994) 301.
[4] K. Nogita, K. Une, J. Nucl. Mater. 226 (1995) 302.
[5] K. Hayashi, H. Kikuchi, K. Fukuda, J. Alloys and Compounds 213&214 (1994) 351.

[6] K. Hayashi, H. Kikuchi, K. Fukuda, J. Nucl. Mater. 248 (1997) 191.
[7] D.R. Lide (Ed.), CRC Handbook of Chemistry and Physics, 73rd ed., CRC, Boca Raton, FL, 1992, pp. 10–293/10–295.
[8] K. Nakata, S. Kasahara, S. Shimanuki, Y. Katano, H. Ohno, J. Kuniya, J. Nucl. Mater. 179–181 (1991) 403.
[9] S.J. Zinkle, J. Nucl. Mater. 191–194 (1992) 645.
[10] F.F. Ziegler, J.P. Biersak, U.L. Littmark, The Stopping and Range of Ions in Solids, Pergamon Press, New York, 1985.
[11] A. Höh, Hj. Matzke, J. Nucl. Mater. 48 (1973) 157.
[12] M. Toulemonde, C. Dufour, E. Paumier, Phys. Rev. B 46 (1992) 14362.
[13] T. Wiss, Hj. Matzke, C. Trautmann, M. Toulemonde, S. Klaumunzer, Nucl. Instrum. and Meth. B 122 (1997) 593.
[14] A. Danlop, D. Lesueur, A. Barbu, J. Nucl. Mater. 205 (1993) 426.
[15] D. Lesueur, A. Danlop, Shim 92, Radiat. Eff. Def. Solids 126 (1993) 163.
[16] M. Amaya, M. Hirai, T. Kubo, Y. Korei, J. Nucl. Mater. 231 (1996) 29.
[17] K. Nogita, K. Une, J. Nucl. Sci. Technol. 30 (9) (1993) 900.
[18] J.H. Davies, F.T. Ewart, J. Nucl. Mater. 41 (1971) 143.
[19] M.J. Bloch, J. Nucl. Mater. 2 (1961) 237.
[20] N. Nakae, A. Harada, T. Kirihara, J. Nucl. Mater. 71 (1978) 314.
[21] A.D. Whapham, Philos. Mag. 26 (1967) 399.
[22] A.D. Whapham, B.E. Sheldon, Philos. Mag. 12 (1965) 1179.
[23] S.J. Zinkle, J. Nucl. Mater. 219 (1995) 113.